A Multiscale Method Modeling Surface Texture Effects

Article *in* Journal of Tribology · April 2007

DOI: 10.1115/1.2540156

4 authors, including:

Ron Van Ostayen
Delft University of Technology
82 PUBLICATIONS **772** CITATIONS

A Multiscale Method Modeling Surface Texture Effects

Alex de Kraker[1]
e-mail: a.dekraker@tudelft.nl

Ron A. J. van Ostayen

A. van Beek

Laboratory of Tribology,
Department of Precision & Microsystems Engineering,
Faculty of 3mE,
Delft University of Technology,
Delft 2628 CD, The Netherlands

Daniel J. Rixen
Engineering Dynamics,
Department of Precision & Microsystems Engineering,
Faculty of 3mE,
Delft University of Technology,
Delft 2628 CD, The Netherlands

*In this paper a multiscale method is presented that includes surface texture in a mixed lubrication journal bearing model. Recent publications have shown that the pressure generating effect of surface texture in bearings that operate in full film conditions may be the result of micro-cavitation and/or convective inertia. To include inertia effects, the Navier–Stokes equations have to be used instead of the Reynolds equation. It has been shown in earlier work (de Kraker et al., 2006, Tribol. Trans., in press) that the coupled two-dimensional (2D) Reynolds and 3D structure deformation problem with partial contact resulting from the soft EHL journal bearing model is not easy to solve due to the strong nonlinear coupling, especially for soft surfaces. Therefore, replacing the 2D Reynolds equation by the 3D Navier–Stokes equations in this coupled problem will need an enormous amount of computing power that is not readily available nowadays. In this paper, the development of a micro–macro multiscale method is described. The local (micro) flow effects for a single surface pocket are analyzed using the Navier–Stokes equations and compared to the Reynolds solution for a similar smooth piece of surface. It is shown how flow factors can be derived and added to the macroscopic smooth flow problem, that is modeled by the 2D Reynolds equation. The flow factors are a function of the operating conditions such as the ratio between the film height and the pocket dimensions, the surface velocity, and the pressure gradient over a surface texture unit cell. To account for an additional pressure buildup in the texture cell due to inertia effects, a pressure gain is introduced at macroscopic level. The method also allows for microcavitation. Microcavitation occurs when the pressure variation due to surface texture is larger than the average pressure level at that particular bearing location. In contrast with the work of Patir and Cheng (1978, J. Lubrication Technol., **78**, pp. 1–10), where the microlevel is solved by the Reynolds equation, and the Navier–Stokes equations are used at the microlevel. Depending on the texture geometry and film height, the Reynolds equation may become invalid. A second pocket effect occurs when the pocket is located in the moving surface. In mixed lubrication, fluid can become trapped inside a pocket and squeezed out when the pocket is running into an area with higher contact load. To include this effect, an additional source term that represents the average fluid inflow due to the deformation of the surface around the pocket is added to the Reynolds equation at macrolevel. The additional inflow is computed at microlevel by numerical solution of the surface deformation for a single pocket that is subject to a contact load. The pocket volume is a function of the contact pressure. It must be emphasized that before ready-to-use results can be presented, a large number of simulations to determine the flow factors and pressure gain as a function of the texture parameters and operating conditions have yet to be done. Before conclusions can be drawn, regarding the dominanant mechanism(s), the flow factors and pressure gain have to be added to the macrobearing model. In this paper, only a limited number of preliminary illustrative simulation results, calculating the flow factors for a single 2D texture geometry, are shown to give insight into the method.* [DOI: 10.1115/1.2540156]

Keywords: surface texture, multiscale method, flowfactor, Reynolds equation, Navier–Stokes, mixed lubrication, finite element method

Introduction

In the last decade, surface texture effects have been studied with growing interest [5–14]. It is observed from experimental studies that surface texture has a positive effect on load capacity and coeffecient of friction for certain applications and load cases [5]. The mechanisms that were pointed out to be responsible for generating additional load capacity are *microcavitation* [6–10], *convective inertia* [13,14] and *piezo viscosity*.

Microcavitation plays a role when subsequent converging and diverging parts of the film cause a pressure fluctuation that is larger than the average pressure level at that particular bearing location. In conformal soft contacts, such as polymer journal bearings, microcavitation may appear. It will be shown in this paper that the occurance strongly depends on the ratio between pocket depth and nominal film height. When the full Navier–Stokes equations are applied at the microlevel, the mass-conservative cavitation algorithm proposed by Brajdic et al. [12] can be used. If the film height and texture geometry is such that the Reynolds equation is valid, microcavitation can be treated numerically by the half-Sommerfeld or by the Reynolds cavitation boundary condition. Whatever method is used to deal with cavitation at microlevel, a pressure correction and flow factors can be derived and added to the macrolevel.

[1]Corresponding author.

Contributed by the Tribology Division of ASME for publication in the JOURNAL OF TRIBOLOGY. Manuscript received March 22, 2006; final manuscript received December 22, 2006. Review conducted by Ilya I. Kudish. Paper presented at the STLE/ASME 2006 International Joint Tribology Conference (TRIB2006), San Antonio, TX, USA, October 22–25, 2006.

Recent publications [13,14], where the Navier–Stokes equations were solved for the flow between two parallel surfaces (one smooth, one having a single surface pocket), have shown that, apart from possible local cavitation, the pressure generating effect of surface texture in full film operation may result from convective inertia. Therefore the generally used Reynolds equation cannot be applied to this problem since the convective inertia forces have been dropped in its derivation from the Navier–Stokes equations.

Piezoviscosity may play a role in heavily loaded oil lubricated contacts where in local converging regions, the pressure rise may be larger than the pressure drop in diverging regions. This effect is unimportant in journal bearing applications where typical pressure levels up to only a few MPa are found.

Another mechanism that has not been previously identified is the *pocket squeeze effect*. In mixed lubrication, the fluid may become trapped inside the pocket. Further loading of the bearing surface when the pocket runs into the contact zone will load the fluid in the pocket and eventually force the fluid to be partially squeezed out.

Flow effects, including microcavitation, and the pocket squeeze effect will affect the performance of the journal bearing system. To analyze the net effect of a particular surface texture, it is not sufficient to study the local effects, but they have to be included into the macroscopic problem to evaluate the overall effect. In Ref. [1] a numerical method has been presented for solving the coupled Reynolds-structure deformation equations in elastic journal bearing problems with partial contact. In the first section of this paper, this model will be reviewed shortly. Flow factors, correcting for the flow resistance induced by a pocket, are introduced in a modified macrolevel Reynolds equation. These flow factors are derived by comparing the numerical solution of the Navier–Stokes equations on a unit control volume with the solution for the 2D Reynolds equation on a smooth unit control area.

An additional source term is included in the macrolevel Reynolds equation, reflecting the fluid volume that is squeezed by a pocket if the surfaces make contact. The volume change of the pocket can be calculated from numerical solution of the linear structure deformation equations for a unit part of the surface containing a single pocket. The pocket-squeeze term is assumed to be a function of the bearing contact pressure only.

Problem Formulation and Equations

In Ref. [1], a numerical solution method was presented for the soft elastohydrodynamic journal bearing problem, including partial contact. An iterative numerical method was used, based on succesive solution of the three-dimensional (3D) structure deformation equations and the 2D Reynolds equation by finite elements. The 2D Reynolds equation was solved first

$$\frac{\partial}{\partial x}\left[\frac{h_t^3}{12\eta}\frac{\partial p_f}{\partial x}+\frac{(U_1+U_2)h_t}{2}\right]+\frac{\partial}{\partial y}\left(\frac{h_t^3}{12\eta}\frac{\partial p_f}{\partial y}\right)=0 \tag{1}$$

with p_f the fluid pressure and h_t the *effective film height*. U_1 and U_2 denote the upper surface and lower surface velocity, respectively. We assume one of the surfaces to be stationary: $U_2=0$. Partial contact was taken into account by a stochastic contact model, first published by Chengwei and Linqing [2]. Asperity contacts were assumed to deform plastically. The effective film height h_t and the contact pressure p_c are a function of the nominal film thickness h only [1]

$$\frac{h_t}{S_q}=\frac{1}{2}\frac{h}{S_q}\left[1+\mathrm{erf}\left(\frac{1}{\sqrt{2}}\frac{h}{S_q}\right)\right]+\frac{1}{\sqrt{2\pi}}e^{-1/2(h/S_q)^2} \tag{2}$$

$$p_c=H\bar{a}_c=\frac{H}{2}\left[1-\mathrm{erf}\left(\frac{1}{\sqrt{2}}\frac{h}{S_q}\right)\right] \tag{3}$$

with S_q the combined root-mean-square surface roughness and H the hardness of the bearing material. The effective film height expresses the average fluid volume between a pair of rough surfaces divided by the total surface area. Details can be found in Refs. [1,2,15]. With the pressure solutions p_f and p_c, the 3D structure deformation equations were solved to find the bearing deformation. Then the film height was updated by the solution for the normal bearing surface deformation u_z

$$h=c+e\cos\phi-u_z \tag{4}$$

with c the radial clearance between the journal and the bearing and e the excentricity. With the new film height h, h_t was computed and the Reynolds equation was solved again. This procedure was repeated until convergence was obtained. Numerical damping was added to the structure deformation equations to stabilize the solution and obtain convergence. The reader is referred to Ref. [1] for further details. The important point here is that we have a macroscopic model that is based on the Reynolds equation.

Micro–macro Coupling: A Modified Reynolds Equation. To introduce the local flow and squeeze effects that result from the presence of a pocket in one of the surfaces in the macroscopic journal bearing model, a modified average Reynolds equation for the macroscopic journal bearing model is proposed

$$\frac{\partial}{\partial x}\left[\phi_{sp,x}\left(-\phi_{px}\frac{h_t^3}{12\eta}\frac{\partial p_f}{\partial x}+\phi_s\frac{U_1 h_t}{2}\right)\right]+\frac{\partial}{\partial y}\left[\phi_{sp,y}\left(-\phi_{py}\frac{h_t^3}{12\eta}\frac{\partial p_f}{\partial y}\right)\right]=Q_s \tag{5}$$

A characteristic property of the micro–macro approach is that microlevel properties are represented at macrolevel in a homogenized way. Clearance variation is a macrolevel property and is taken into account at macrolevel instead of microlevel. At microlevel a constant film height equal to the film height $h(x,y)$ at macrolevel can be assumed, as long as the number of texture unit cells is large. For a couple of bearing surface, one smooth and one having a surface texture, three different operating states can be distinguished as follows:

1. The smooth surface moves, the textured surface is stationary;
2. The textured surface moves, the smooth surface is stationary; and
3. The smooth surface moves and the textured surface moves.

Equation (5) describes the fluid on the macroscopic level, i.e., for the complete journal bearing problem, replacing Eq. (1), and is valid for Case 1; a smooth moving surface together with a stationary textured surface. Concerning the flow effects, we will restrict the model in this paper to Case 1. For Cases 2 and 3, an additional term will appear in the Reynolds equation, resulting from the fluid that is transported by a moving pocket. In future work, the model will be extended for these cases.

In the presence of a surface texture, the mass flow between the surfaces will differ from a regular nontextured pair of surfaces. To correct the flow, a set of flow factors ϕ is introduced in the Reynolds equation. The factors ϕ_{px} and ϕ_{py} are pressure flow factors and ϕ_s is a shear flow factor. These flow factors are determined at a microscopic level, i.e., at a small representative piece of surface containing the important features of the surface texture. Only a small part of the surface area of this unit cell is covered by the surface pocket itself, such that the flow is assumed to be fully developed at its boundaries. In the Navier–Stokes simulations, it was found that the flow profile at the boundaries of the unit cell was unaffected by the presence of the pocket and was a linear combination of Poiseuille and Couette flow at a pocket ratio of 0.3. It is assumed that the bearing surface contains a large number of surface pockets such that the effects may be averaged in space.

The pressure flow factors ϕ_{px} and ϕ_{py} are determined for pure pressure induced flow, i.e., the surface velocity is equal to zero and hence

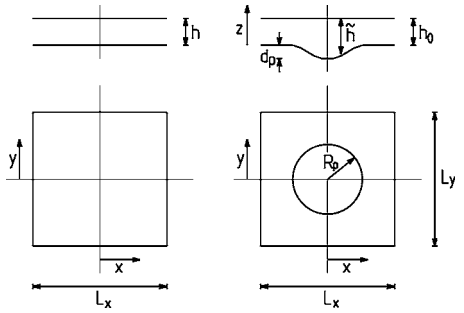

Fig. 1 GUFC (*a*) and TUFC (*b*)

$$\phi_{px} = \phi_{px}(\partial p/\partial x, \text{geometry}) \tag{6}$$

$$\phi_{py} = \phi_{py}(\partial p/\partial y, \text{geometry}) \tag{7}$$

The shear flow factor ϕ_s is determined for pure shear flow conditions

$$\phi_s = \phi_s(U_1, \text{geometry}) \tag{8}$$

The shear flow factor is a function of the upper surface velocity U_1 ($U_2=0$). This method appears to be similar to the classical flow factor method of Patir and Cheng [3]. However, it differs from their method in the way the flow factors are determined. In the work of Patir and Cheng, the Reynolds equation was used to solve the flow through a rough unit piece of control volume. Hence, the pressure flow factor ϕ_{px} is a function of $\partial p/\partial x$ and geometrical properties only, but not of U, nor $\partial p/\partial y$. This is due to the fact that the flow according to the Reynolds equation is a linear combination of pressure induced flow and shear driven flow. This is not the case for the flow in a deterministic texture unit cell. In Arghir et al. [13] and Sahlin et al. [14] it was shown that the Navier–Stokes equations must be used in general. Therefore, the flow is no longer a linear combination of pressure—and shear flow and additional corrections $\phi_{\text{sp},x}(\partial p/\partial x, \partial y/\partial x, U_1, \text{geometry})$ and $\phi_{\text{sp},y}(\partial p/\partial x, \partial y/\partial x, U_1, \text{geometry})$ are necessary.

This description, splitting up the flow factors, has the advantage that it becomes clear immediately if there is any crosscoupling between the pressure flow resistance and the shear flow velocity or between the shear flow resistance and the pressure gradient over a unit cell with surface texture. If the factor $\phi_{\text{sp},x}(\partial p/\partial x, \partial p/\partial y, U, \text{geometry})$ is equal to unity there is no cross coupling.

The additional source term Q_s (m/s) in Eq. (5) reflects the average additional fluid inflow per unit surface area, resulting from the pocket-squeeze effect. The pocket-squeeze effect is the result of surface deformation, reducing the volume of the surface pocket. This effect is present if the textured surface is nonstationary and is significant in mixed lubrication only, i.e., when the surfaces make contact.

Summarizing, the correction factors ϕ_{px}, ϕ_{py}, ϕ_s, $\phi_{\text{sp},x}$, and $\phi_{\text{sp},y}$, stem from flow effects due to the presence of a surface texture and Q_s results from the pocket-squeeze effect. The following sections will address the pocket flow effect and determination of the flow factors and pocket-squeeze effect, respectively.

Pocket Flow Effect

In the macroscopic journal bearing model, the details of the surface pocket cannot be represented. For a surface with a simple texture, we can define a representative unit cell that contains a single surface pocket. In Fig. 1(*a*), the macroscopic representation of a (global) unit flow cell (GUFC) is shown. The right figure shows the texture unit flow cell (TUFC) representing the details of the pocket shape. To derive the flow correction factors ϕ_{px},ϕ_{py}, and ϕ_s, we compare the solutions for the TUFC and the GUFC in terms of the mass flow through the cell. For the GUFC, we use the 2D Reynolds equation to determine the flow. For the TUFC, the Navier–Stokes equations are used to solve for the flow and pressure field. In the next sections, we will adress the calculation of the flow factors, illustrated by 2D examples. Note that at the microscale, the surfaces are nominally flat since the radius of the bearing $R >> L_x, L_y$. The surface velocities and pressure gradients in the calculations presented in this paper were chosen such as they appear in journal bearing applications.

Microcavitation. Microcavitation can occur when the amplitude of the pressure variation, induced by the surface texture, is larger than the nominal pressure level at that particular location in the bearing. Hence, the pressure solution at micro-level must be compared to the pressure at macro-level.

In Fig. 2, the pressure solution is shown for the TUFC at different nominal film height. From top to bottom, the ratio h_0/d_p is varied from 10 down to 0.01. The problem is solved both by the Navier–Stokes equations and by the Reynolds equation. For a film height that is in the order of or larger than the maximum pocket depth, a large difference in pressure solution is found. This is due to *convective inertia*. The amplitude of the pressure variation is relatively small and will, depending on the bearing pressure at macrolevel, probably not lead to microcavitation. For a film height that is small compared to the maximum pocket depth, the contribution of convective inertia becomes negligible and the Reynolds equation can be used. The amplitude of the pressure solution is large, due to the so-called ram effect: a rapidly converging restriction from the pocket to the thin film. From these figures, it can be concluded that microcavitation occurs when the film height is small compared to the pocket depth and that, in this case, the Reynolds equation is accurate. For $h_0/d_p \geqslant 1$, convective inertia plays a dominant role and microcavitation is not likely to occur since the amplitude of the pressure variation remains small. The amplitude of the pressure variation is about 0.25 MPa for the case where $h_0/d_p=0.01$. This pressure variation may exceed the pressure level in a journal bearing and lead to microcavitation. Let us assume the fluid pressure at the location of the TUFC at the macrolevel p_f to be 0.1 MPa. Either the half-Sommerfeld cavitation boundary condition or the Reynolds cavitation boundary condition can be used. The first can be implemented by simply ignoring the negative part of the pressure solution and set it to zero. The Reynolds cavitation boundary condition is implemented by succesive iteration of the resticted ($p_{\text{TUFC}}+p_f \geqslant 0$) problem. Figure 3 shows that both methods give similar results. The use of the half-Sommerfeld boundary condition is preferable, since this method can be implemented by simply computing the pressure solution at microlevel as a function of the nominal film height h_0 and pass on this information to the macrolevel. At the macrolevel (where the p_f is known), the half-Sommerfeld boundary condition is applied to the microlevel solution and the average pressure and load capacity can be corrected. Applying the Reynolds cavitation boundary condition requires communication between micro- and macrolevel and vice versa. An alternative that needs computing power, is to use the Navier–Stokes equations and implement the cavitation model that was used in Brajdic et al. [12]. As long as the ratio h_0/d_p is such that the Reynolds equation is valid, which is the case for texture geometries that possibly result in cavitation, the Reynolds based method should be sufficient. It would however be very interesting to compare the cavitation methods based on the Reynolds equation to the Navier–Stokes cavitation model proposed by Brajdic et al.

The two cavitation methods discussed above are not mass conservative and, hence, an error is made at microlevel. This error is, however, resticted to the microlevel and the macromodel can still be mass conservative. This is an advantage that is inherent to the micro–macro approach. Application of the Reynolds cavitation boundary condition to a *row* of surface texture cells, as done in Ronen et al. [7] will give inaccurate results and overestimate the

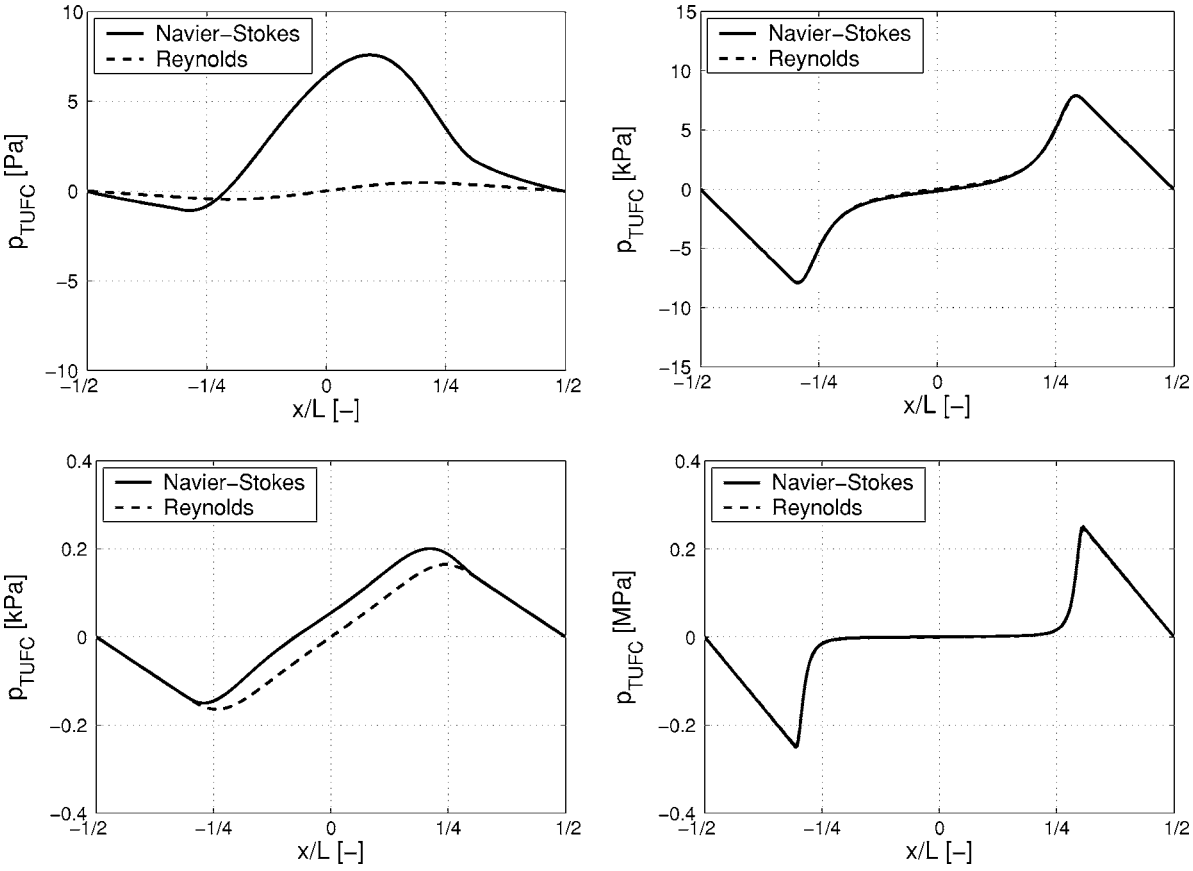

Fig. 2 Pressure distribution at the upper surface of the TUFC for pure shear driven flow (U_1=1 m/s) for different h_0/d_p ratio (from top to bottom: 10, 1, 0.1, 0.01). Note the different *y* axis scaling.

load capacity due to microcavitation. At each of the successive reformation boundaries, mass conservation is violated. In a numerical sense, mass is added to the system in each cavitation area resulting in a large accumulated error. This is not the case for the micro–macro approach.

Calculation of ϕ_{px} and ϕ_{py}. To calculate the pressure flow factor in x direction, ϕ_{px}, periodical boundary conditions with respect to the the three components of the velocity are prescribed on boundaries a and b of the TUFC (Fig. 4). A commercially available finite-element code, called SEPRAN [4], is used to discretize the Navier–Stokes equations on the TUFC domain. A fully incompressible formulation (Q_1-P_0) is used, where both the velocities and the pressure are considered as unknowns. The solution is constrained by a prescribed mass flux. The pressure solution is then fixed up to an additive constant. To fix the pressure solution, the pressure must be set in one point of the domain: for example $p=0$ at the upper outflow corner. The side boundaries are no-flow boundaries, i.e., the normal velocity componenent v_y equals zero for the case $\partial p/\partial y=0$. The surface velocity U_1 is set to zero. The mass flow through the TUFC is given by

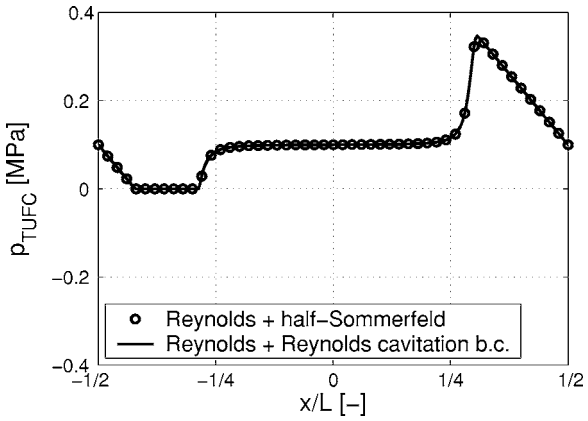

Fig. 3 Pressure distribution at the upper surface of the TUFC for shear driven flow (U_1=1 m/s) and h_0/d_p=1/100 solved from the Reynolds equation with different cavitation boundary conditions

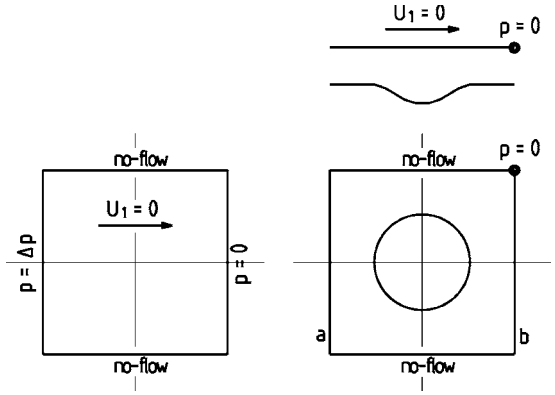

Fig. 4 Computational domain for the 2D GUFC (*a*) and for the 3D TUFC (*b*) with suitable boundary conditions for calculation of ϕ_{px}. Boundaries *a* and *b* are periodical in terms of the velocity field.

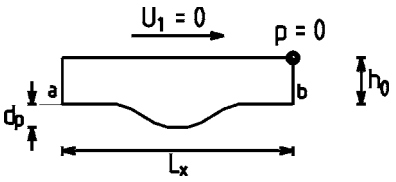

Fig. 5 2D TUFC geometry. Boundary *a* and *b* are periodic in terms of the velocity field. The nominal film height $h_0 << L_x$.

$$Q_{\mathrm{TUFC}} = \rho \int_{\Omega_a} v_{\perp}^{a}\, d\Omega_a \tag{9}$$

with Ω_a the area of the inflow boundary and $v_{\perp}^{a}$ the velocity inward normal to this boundary. The Reynolds equation is valid on the 2D GUFC domain, shown in Fig. 4(*a*). The pressure at the upper inflow corner, Δp, that was found from the pressure solution for the TUFC, is prescribed as an essential boundary condition for the GUFC problem at the inflow boundary. No-flow boundary conditions are also used at the side boundaries. The mass flow through the GUFC can be calculated

$$Q_{\mathrm{GUFC}} = \rho \int_{-L_y/2}^{L_y/2} \left(-\frac{h_t^3}{12\eta}\frac{\partial p}{\partial x} + \frac{U_1 h_t}{2} \right) dy \tag{10}$$

Since, for pure pressure induced flow, the surface velocity $U_1 = 0$, the second term equals zero and the flow through the GUFC for can be calculated from

$$Q_{\mathrm{GUFC}}(U_1 = 0) = -L_y \frac{\rho h_t^3}{12\eta}\frac{\partial p}{\partial x} \tag{11}$$

The pressure flow factor in x direction is

$$\phi_{px} = \frac{Q_{\mathrm{TUFC}}(U_1 = 0)}{Q_{\mathrm{GUFC}}(U_1 = 0)} \tag{12}$$

The derivation of the pressure flow factor ϕ_{py} in y direction is very similar. For a x-y symmetric TUFC (as shown in Fig. 4), the flow factor ϕ_{py} is actually identical to ϕ_{px}.

Calculation of ϕ_{px}: 2D Simulation Results. Some preliminary results for the 2D case are shown in Fig. 8. The geometry for the 2D TUFC is based on a squared cosine shape and is shown in Fig. 5. The boundaries a and b are periodic in terms of the velocity field. The nominal film height $h_0 = L_x/100$, with the length of the cell $L_x = 9$ mm. The nominal film height h_0 is chosen to be equal to the maximum pocket depth d_p. The viscosity and density of the fluid are set to 10^{-3} and 10^{3}, respectively.

The pressure distribution at the upper surface, solved from the Navier–Stokes equations, is represented by the solid curve in Fig. 6. The solution for the TUFC that would be found by the Reynolds equation is given by the dotted curve and is antisymmetric around the linear pressure drop over the GUFC (macrosmooth representation of the unit cell). Both the Navier–Stokes solution and the Reynolds solution have a steeper pressure gradient at the inlet (at $x = -L/2$), compared to the macropressure gradient. Therefore, the flow resistance is less in the presence of a surface pocket, compared to a smooth surface and the flow factor $\phi_{px} > 1$. As a result from this, the pressure build up in the textured journal bearing problem will be *less effective*. However, it is clear from Fig. 6 that load carrying capacity is generated by the asymmetric pressure distribution in the TUFC. To account for this effect in the macroscopic bearing problem, a *load correction* is introduced in one of the next sections. Both effects have to be included in the journal bearing problem to decide whether the total effect has a positive or negative influence on load carrying capacity and friction in a journal bearing. Surface texture design parameters can then be optimized to obtain the largest load carrying capacity or the lowest friction.

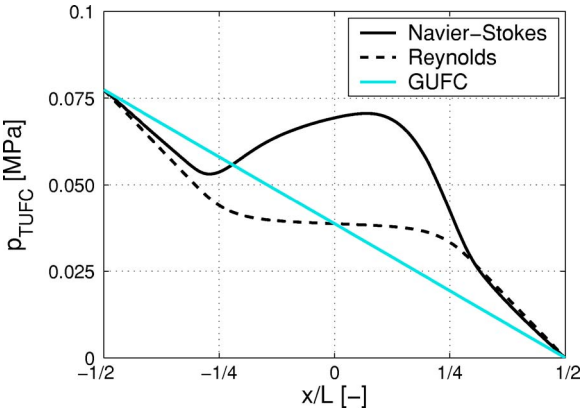

Fig. 6 Pressure distribution at the upper surface for pure pressure induced flow. The solid curve represents the solution when the Navier–Stokes equations are used; the dotted curve gives the Reynolds solution. The linear curve is the solution for the macroscopic (smooth) representation of the unit cell, the GUFC.

Streamlines for the solution shown in Fig. 6 are shown in Fig. 7(*b*). A recirculation zone is not seen yet, but the streamlines are clearly asymmetric. The additional load carrying capacity that is generated appears to be related to the amount of streamline asymmetry.

In Fig. 8 the pressure distribution at the upper surface of the TUFC is shown for pure pressure driven flow at different Reynolds number. The Reynolds number is defined as $\mathrm{Re} = \rho h_0 v_{x,\max}/\eta$. The larger the Reynolds number and the larger the pressure drop over the TUFC, the more nonsymmetric the pressure distribution becomes and the larger the contribution of convective inertia. Meanwhile, for increasing pressure drop over the TUFC, the pressure flow factor ϕ_{px} drops to slightly lower values as shown in Fig. 9. The dotted line gives the flow factor ϕ_{px} calculated by using the Reynolds equation to solve the TUFC problem.

Note that for Re approaching a value of 1000, the flow becomes turbulent and the results presented here may loose their validity.

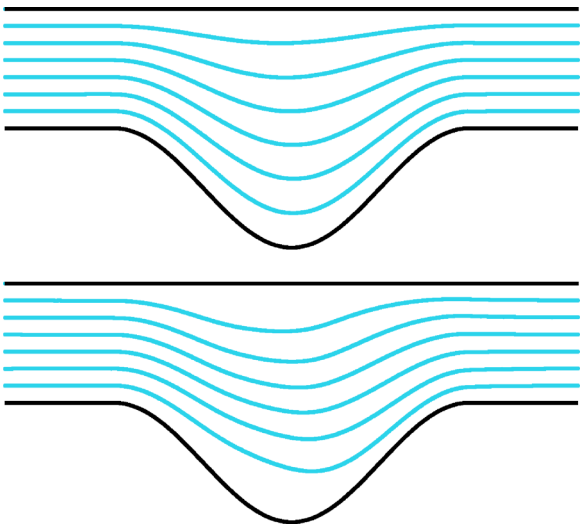

Fig. 7 Streamlines for pure pressure induced flow at $\partial p/\partial x = -1$ MPa/m (*a*) and $\partial p/\partial x = -8.5$ MPa/m (*b*) correspond to the solution in Fig. 6

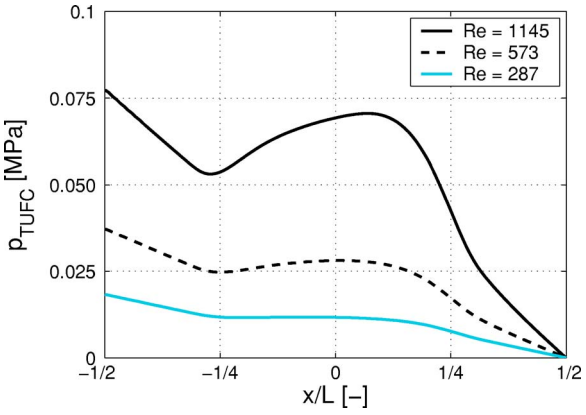

Fig. 8 Pressure distribution at the upper surface of the TUFC for pure pressure induced flow (U_1=0 m/s) at different Reynolds numbers

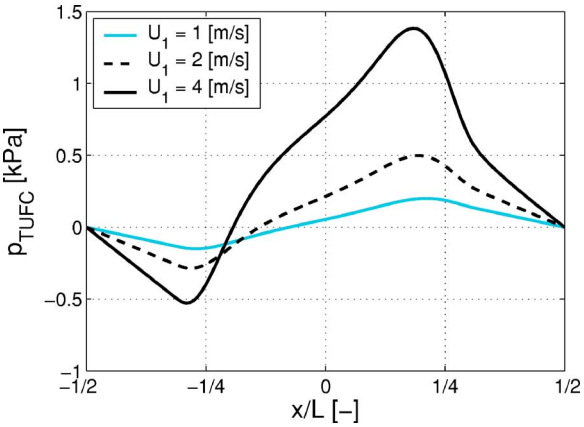

Fig. 11 Pressure distribution at the upper surface of the TUFC for pure shear boundary conditions at different Reynolds numbers

Calculation of ϕ_s. Calculation of the shear flow factor is similar to the method that was used to determine the pressure flow factors. Suitable boundary conditions for this problem are shown in Fig. 10. Periodical boundary conditions are prescribed for the velocity component and also for the pressure this time. To fix the pressure solution, zero pressure is prescribed in one corner of the TUFC.

The shear flow factor ϕ_s is calculated using Eq. (12), as previously used for the calculation of ϕ_{px}, however with different boundary conditions

$$\phi_s = \frac{Q_{\mathrm{TUFC}}(\partial p/\partial x = 0)}{Q_{\mathrm{GUFC}}(\partial p/\partial x = 0)} \tag{13}$$

The mass flow Q_{TUFC} has been defined in Eq. (9). For the pure shear boundary conditions, the mass flow through the GUFC is

$$Q_{\mathrm{GUFC}}(\partial p/\partial x = 0) = L_y \frac{U_1 h_t}{2} \tag{14}$$

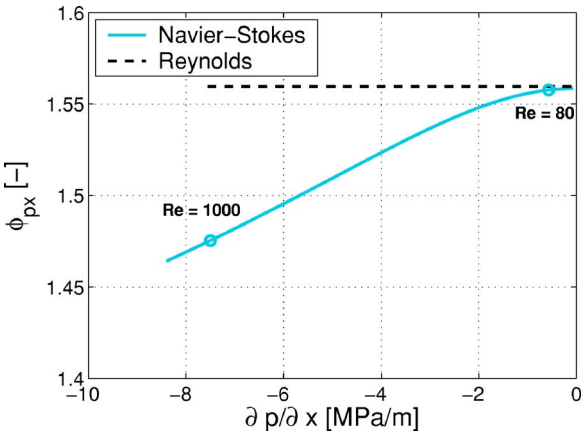

Fig. 9 Pressure flow factor ϕ_{px} as a function of the pressure gradient over the TUFC

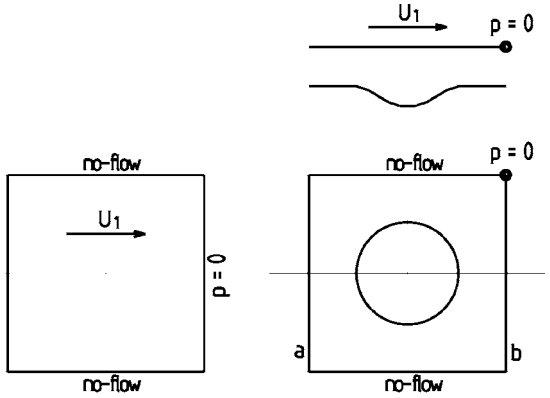

Fig. 10 Computational domain for the 2D GUFC (*a*) and for the 3D TUFC (*b*) with suitable boundary conditions for calculation of ϕ_s. The boundaries *a* and *b* are periodical, both for the velocity variables and the pressure.

Calculation of ϕ_s: 2D Simulation Results. For the 2D case the same boundary conditions were used as we used for the calculation of ϕ_{px} in 2D as shown in Fig. 5, except for the upper surface velocity U_1. Furthermore, periodical boundary conditions with respect to the pressure are necessary at boundaries *a* and *b*. Again, the pressure must be fixed in one point in the domain. In Fig. 11, the pressure solution at the upper smooth surface for pure shear driven flow is shown. The surface velocities U_1 are 1, 2 and 4 m/s, respectively. For the lowest velocity, the pressure distribution is almost antisymmetric and approaches the Reynolds solution. For increasing surface velocity (Re number) the pressure distribution tends to become more asymmetric. Please note that the pressure amplitude is two orders of magnitude smaller compared to Fig. 8. In Fig. 12, streamlines are plotted for the pure shear driven flow at surface velocity U_1=4 m/s. A large slightly asymmetric recirculation zone is located inside the pocket.

The shear flow factor is displayed as a function of the surface velocity U_1 in Fig. 13. For low surface velocity, the flow factor approaches the Reynolds limit. At increasing surface velocity, the flow factor drops to a lower value again, i.e., the flow resistance increases.

Calculation of $\phi_{\mathrm{sp},x}$ and $\phi_{\mathrm{sp},y}$. The factors $\phi_{\mathrm{sp},x}$ and $\phi_{\mathrm{sp},y}$ take into account how the flow resistance is affected by a combination of a moving surface and a pressure gradient over the TUFC. Instead of no-flow boundary conditions in y direction, a mass flow in y direction must also be prescribed. The pressure gradient $\partial p/\partial y$ follows from the solution. For the flow in x direction holds

$$\phi_{\mathrm{sp},x} = \frac{Q_{\mathrm{TUFC}}(U_1, \partial p/\partial x, \partial p/\partial y)}{\phi_{px} Q_{\mathrm{GUFC}}(U_1 = 0) + \phi_s Q_{\mathrm{GUFC}}(\partial p/\partial x = 0)} \tag{15}$$

The y-flow correction factor $\phi_{\mathrm{sp},y}$ shows how the flow resistance in y direction is affected by a surface velocity U_1 and pressure gradient in x direction

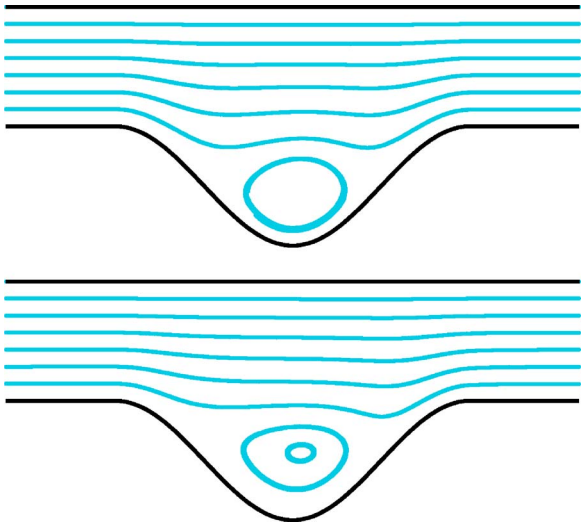

Fig. 12 Streamlines at pure shear driven flow: (top) U_1 =1 m/s; (bottom) U_1=4 m/s. A slightly asymmetric recirculation zone is located inside the pocket for increasing surface velocity.

$$\phi_{\mathrm{sp},y} = \frac{Q_{\mathrm{TUFC},y}(U_1, \partial p/\partial x, \partial p/\partial y)}{\phi_{py} Q_{\mathrm{GUFC},y}(U_1 = 0)} \tag{16}$$

Calculation of $\phi_{\mathrm{sp},x}$: 2D Simulation Results. The flow factor $\phi_{\mathrm{sp},x}$ represents how the flow resistance in x direction depends on a combination of a surface velocity U_1, a pressure gradient $\partial p/\partial x$ and a pressure gradient $\partial p/\partial y$. In Fig. 14, the results are shown for the 2D TUFC of Fig. 5. The factor $\phi_{\mathrm{sp},x}$ is displayed as a function of the pressure gradient $\partial p/\partial x$ at different surface velocity U_1. For increasing pressure gradient and increasing surface velocity, an increasing flow resistance is found ($\phi_{\mathrm{sp},x} < 1$).

The solution for the marked point in Fig. 14 is shown in Figs. 15 and 16. Again, an asymmetric recirculation zone is located inside the pocket.

Pressure Gain. The bearing pressure at macrolevel is given by [1]

$$p = p_c + p_f \tag{17}$$

with p_c the contact pressure and p_f the fluid pressure. Two mechanisms have been pointed out contributing to the pressure generating effect of surface texture in full film lubrication, i.e., convec-

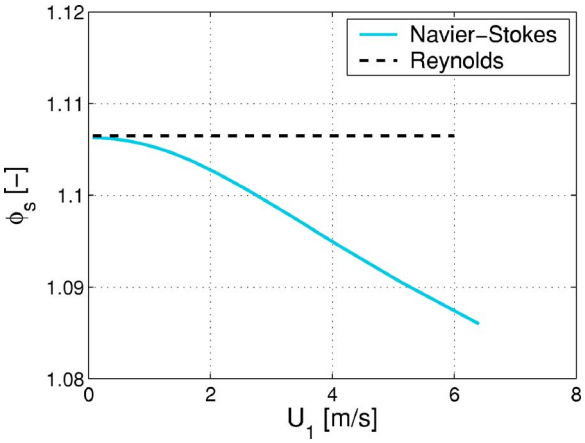

Fig. 13 Shear flow factor ϕ_s as a function of the upper surface velocity U_1

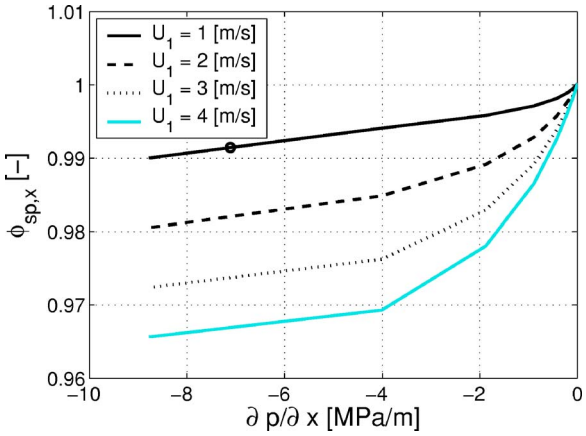

Fig. 14 Pressure flow factor $\phi_{\mathrm{sp},x}$ as a function of the pressure drop over the TUFC for different surface velocities

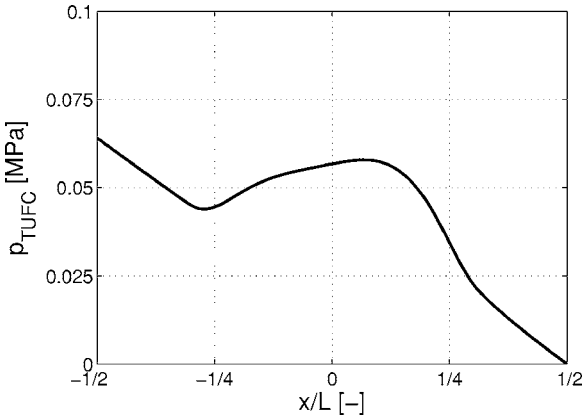

Fig. 15 Pressure distribution at the upper surface of the TUFC. Operating conditions: U_1=1 m/s, $\partial p/\partial x$=–7.1 MPa/m

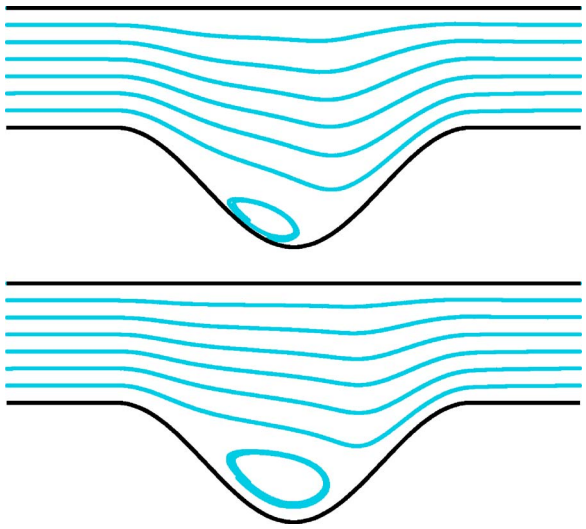

Fig. 16 Streamlines for a flow that is driven both by an upper surface velocity U_1 and pressure gradient over the TUFC. Operating conditions: $\partial p/\partial x$=–7.1 MPa/m, U_1=1 m/s (*a*), U_1 =4 m/s (*b*).

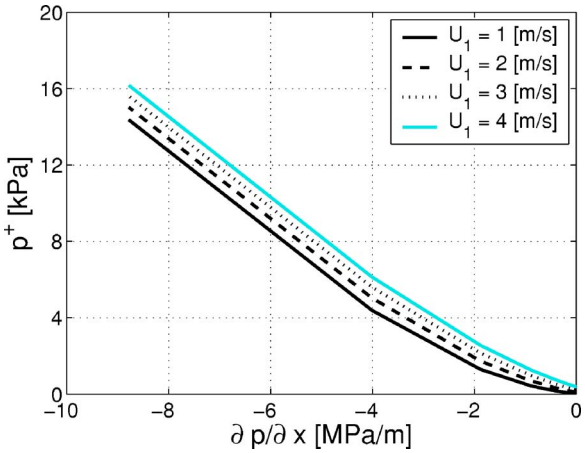

Fig. 17 Pressure gain as result of convective inertia as a function of the pressure gradient for different surface velocities

tive inertia effects and microcavitation. Both phenomena result in an asymmetric pressure distribution over the TUFC. Therefore, the average pressure at macrolevel is incorrect and has to be modified

$$p = p_c + p_f + p^+ \tag{18}$$

with p^+ an additional pressure gain

$$p^+ = \frac{1}{L_x L_y}\int_\Omega \max(p_f + p_{\mathrm{TUFC}}, 0)\, d\Omega - p_f \tag{19}$$

with the term under the integral the pressure solution with half-Sommerfeld cavitation boundary condition. Hence, p^+ is not only a function of the TUFC geometry, $\partial p/\partial x$ and $\partial p/\partial y$ at macrolevel, but also of the average pressure at macrolevel p_f. Figure 17 shows how the pressure gain p^+ as a result of convective inertia only depends on the surface velocity and pressure gradient for the 2D case with $h_0/d_p = 1$.

Pocket Squeeze Effect

Q_s is an additional source term that reflects the average additional fluid inflow per unit surface area, resulting from the pocket-squeeze effect. This effect is present if the textured surface is moving ($U_2 \neq 0$) and deformable. The effect also exists for a moving rigid textured surface in combination with a deformable countersurface. However, this will be less effective. In this section, we restrict ourselves to a moving deformable textured surface. All variables and parameters that related to the microscale and have an equivalent at the macroscale are provided with a tilde, e.g., $\tilde{h}$ denotes the film height at the microscale.

The source term Q_s can also be interpreted as a squeeze term $-d\tilde{h}_{\mathrm{av}}/dt$ with h_{av} the average distance between a unit piece of surface with a pocket and the counter surface

$$\tilde{h}_{\mathrm{av}} = \frac{1}{A}\int_\Omega \tilde{h}\, d\Omega \tag{20}$$

with A the surface area of a unit piece of surface containing a single pocket (see Fig. 18). The average additional fluid inflow Q_s is given by the change of the average height per unit time

$$Q_s = -\frac{\partial \tilde{h}_{\mathrm{av}}}{\partial t} = -\frac{1}{A}\frac{\partial V}{\partial t} = -\frac{1}{A}\frac{\partial V}{\partial x}\frac{\partial x}{\partial t} \tag{21}$$

with V the pocket volume. Replacing $\partial V/\partial x$ by

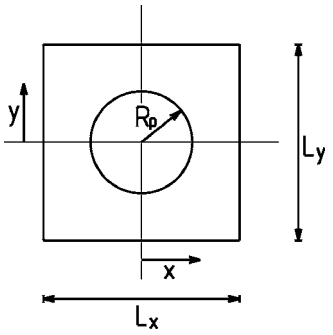

Fig. 18 Surface area of the texture unit cell

$$\frac{\partial V}{\partial x} = \frac{\partial V}{\partial p_c}\frac{\partial p_c}{\partial x} \tag{22}$$

and replacing $\partial x/\partial t$ by the the surface velocity U_2 gives the following expression for Q_s

$$Q_s = -\frac{1}{A}\frac{\partial V}{\partial p_c}\frac{\partial p_c}{\partial x}(U_2) \tag{23}$$

The fraction $\partial V/\partial p_c$ is assumed not to be a function of x, such that this equation can be rewritten

$$Q_s = -\frac{\partial}{\partial x}\left[\frac{\partial V}{\partial p_c}\frac{(U_2)p_c}{A}\right] \tag{24}$$

Substituting this equation into Eq. (6) and rearranging gives the modified Reynolds equation for the macroproblem

$$\frac{\partial}{\partial x}\left(-\phi_{\mathrm{sp},x}\phi_{px}\frac{h_t^3}{12\eta}\frac{\partial p_f}{\partial x} + \phi_{\mathrm{sp},x}\phi_s\frac{U_1 h_t}{2} + \frac{\partial V}{\partial p_c}\frac{U_2 p_c}{A}\right) + \frac{\partial}{\partial y}\left(-\phi_{\mathrm{sp},y}\phi_{py}\frac{h_t^3}{12\eta}\frac{\partial p_f}{\partial y}\right) = 0 \tag{25}$$

The additional source term that appears at the left-hand side is a function of the contact pressure p_c only. The contact pressure is a macroscopic quantity and follows from the solution of the macro-journal bearing model. The factor $\partial V/\partial p_c$ may be a function of the material parameters and the shape of the pocket. In the next section, we show that the factor $\partial V/\partial p_c$ is not a function of the contact pressure p_c itself. The value for $\partial V/\partial p_c$ has to be derived by the solution of a 3D structure deformation problem for a piece of material containing a single pocket: a texture unit deformation cell (TUDC).

Calculation of $\partial V/\partial p_c$. A standard finite-element routine is used to descretise the linear structure deformation equations on the TUDC domain as shown in Fig. 19. The following boundary conditions are used: zero displacement at the bottom surface and zero normal displacement at the side walls. The contact model that was used in Ref. [1] is applied here as well. With h_0 the z coordinate of the counter surface, the distance $\tilde{h}$ between the surfaces is

$$\tilde{h} = h_0 - \tilde{u}_z - \tilde{z}_s \tag{26}$$

with $\tilde{u}_z$ the normal deformation of the surface and $\tilde{z}_s$ the surface z coordinate. Throughout this paper, we use the following function for the shape of the pocket

$$\tilde{z}_s = -d_p \cos\left(\frac{\pi}{R_p}\frac{\sqrt{x^2+y^2}}{2}\right)^2 \quad \forall\, x^2 + y^2 \leq R_p$$

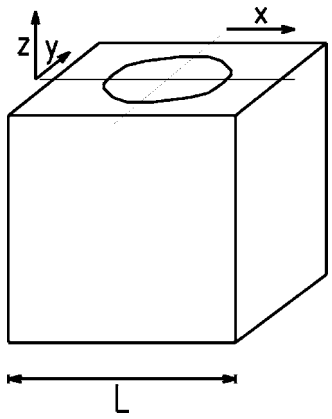

Fig. 19 TUDC: 3D domain for fem solution of structure deformation equations

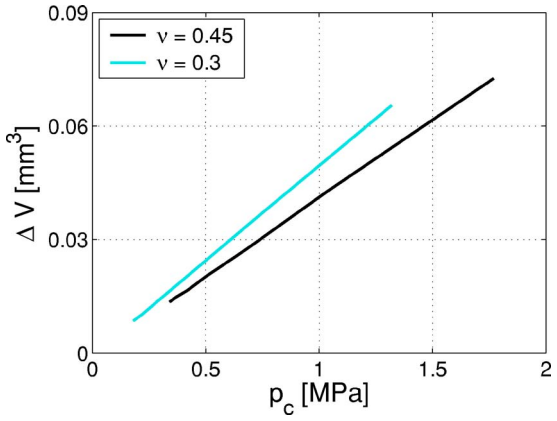

Fig. 21 Numerical solution for the pocket volume change as a function of the average contact pressure

$$\tilde{z}_s = 0 \; \forall \; x^2 + y^2 > R_p \tag{27}$$

with d_p the maximum pocket depth. The pocket shape is illustrated in Fig. 16. For a negative distance $\tilde{h}$, contact occurs. According to the model of Chengwei [2], the effective height between Gaussian distributed rough surfaces is

$$\frac{\tilde{h}_t}{S_q} = \frac{1}{2}\frac{\tilde{h}}{S_q}\left[1 + \mathrm{erf}\left(\frac{1}{\sqrt{2}}\frac{\tilde{h}}{S_q}\right)\right] + \frac{1}{\sqrt{2\pi}} e^{-1/2(\tilde{h}/S_q)^2} \tag{28}$$

with S_q the composite rms surface roughness. We assume a plastic asperity deformation mode, such that the contact pressure follows from Ref. [1]

$$\tilde{p}_c = H\bar{a}_c = \frac{H}{2}\left[1 - \mathrm{erf}\left(\frac{1}{\sqrt{2}}\frac{\tilde{h}}{S_q}\right)\right] \tag{29}$$

To solve this contact problem, a staggered numerical scheme is used, shown in Fig. 20. Artificial damping was used to stabilize the solution. From the solution, we compute the pocket volume change by

$$\Delta V = V_p - V_0 \tag{30}$$

with V_p the final pocket volume and V_0 the original pocket volume.

Pocket Squeeze Effect: Preliminary Simulation Results. Preliminary results for the pocket volume change ΔV as a function of the contact pressuree p_c are shown in Fig. 21. Table 1 lists the dimensions and material parameters that were used. The volume change is found to be a linear function of the contact pressure. This means that the geometric nonlinearity (growing contact area for a smooth pocket shape) is unimportant. From these results, the derivative dV/dp_c can easily be derived. For the examples shown in Fig. 21, the value for dV/dp_c is 0.041 mm^3/MPa and 0.05 mm^3/MPa, respectively. It is also clear from Fig. 21 that dV/dp_c is larger for more compressible materials (ν=0.3). This is due to the fact that the effective stiffness of the TUDC is larger for more incompressible materials.

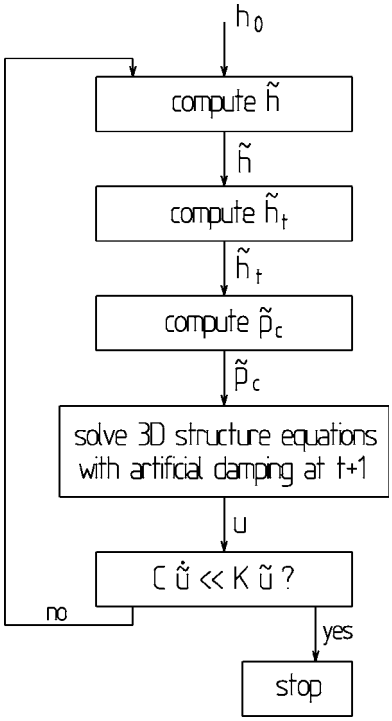

Fig. 20 Numerical scheme

Conclusions

In this paper, a micro–macro multiscale method is presented that includes the effects of surface texture in a macroscopic bearing model. Two effects are included: pocket flow effects and squeezing of the pocket when the surfaces are in contact.

The method including the flow effects is very similar to the flow factor method introduced by Patir and Cheng [3]. The method proposed here differs from that of Patir and Cheng by the equations that are used to solve the flow in the microscopic cell (TUFC in our case). Patir and Cheng used the Reynolds equation for a piece of surface with random roughness height distribution and compared the flow to that for a smooth surface with identical

Table 1 Dimensions and material parameters for the TUDC

Description	Parameter	Value	Dimension
TUDC dimension	L_x	9	(mm)
TUDC dimension	L_y	9	(mm)
TUDC thickness	t	9	(mm)
Pocket area ratio	ξ	0.3	(-)
Pocket depth	d_p	0.045	(mm)
Composite roughness	S_q	0.424	(μm)
Young's modulus	E	1	(GPa)
Poisson ratio	ν	0.45	(-)
Hardness	H	50	(MPa)

average film gap. The method discussed in this work uses the Navier–Stokes equations since convective inertia (that has been dropped in the Reynolds equation) might become important.

The flow factors $\phi_{sp,x}$ and $\phi_{sp,y}$ have to be solved by the Navier–Stokes equations since a relation between pressure flow resistance in x direction and the surface velocity U_1 or pressure gradient $\partial p/\partial y$ cannot be solved from the Reynolds equation. The antisymmetric character of the pressure distribution (that contributes to the load carrying capacity), evolving from the contribution of convective inertia, has to be solved by the Navier–Stokes equations.

It has become clear that for $h_0 \ll d_p$, microcavitation is the dominant flow effect. In this case, the Reynolds equation with half-Sommerfeld boundary conditions appears to be sufficient to solve the microproblem.

Microcavitation and its numerical treatment are subject of further study. It has, however, been shown that the multiscale method proposed in this paper allows us to include a local caviation algorithm. The pressure gain can be calculated as a function of the pressure solution at macrolevel.

For film heights that are in the same order or larger than the pocket depth, the pressure variation is relatively small and cavitation is not likely to occur. In this case, convective inertia effects are important and the Navier–Stokes equations are necessary to solve the problem.

Enclosed surface pockets that come into contact can squeeze out some of the fluid caught in the pocket. The pocket volume change is computed by numerically simulating the deformation of a 3D unit piece of surface, containing a single pocket, that comes into contact with the counter surface. This effect is included at macrolevel by an additional source term.

In future research flow factors, pressure gain (as a result of microcavitation and convective invertia) and pocket squeeze factors will be determined by numerical simulation as a function of the pocket geometry, film height and macroscopic operating conditions such as surface velocity and the global bearing pressure gradient. Implementing these results in the macroscopic bearing model allows us to evaluate the net effect of the surface texuture.

Acknowledgment

This research is supported by the Technology Foundation STW, Applied Science Division of NWO and the technology programme of the Ministry of Economic Affairs.

Nomenclature

A = surface area
$\bar{a}_c$ = contact area fraction
c = radial clearance
d_p = pocket depth
E = Young's modulus
e = eccentricity
H = hardness
$h, \tilde{h}$ = film height
$h_t, \tilde{h}_t$ = effective film height
h_0 = nominal film heigt
p = pressure
$p_c, \tilde{p}_c$ = contact pressure
p_f = fluid pressure
Q = mass flow
R = bearing radius
Re = Reynolds number
R_p = pocket radius
S_q = surface roughness parameter
t = time
U = sum velocity
U_1 = upper surface velocity
U_2 = lower surface velocity
$u_z, \tilde{u}_z$ = normal surface deformation
V = pocket volume
(x, y, z) = Cartesian coordinate system
η = viscosity
ν = Poisson ratio
ϕ = angular journal bearing coordinate
ϕ_{px}, ϕ_{py} = pressure flow factor
ϕ_s = shear flow factor
$\phi_{sp,x}, \phi_{sp,y}$ = flow correction factor
ρ = fluid density
ξ = pocket area ratio

References

[1] de Kraker, A., Ostayen, R. A. J., and Rixen, D. J., 2006, "Calculation of Stribeck Curves for (Water) Lubricated Journal Bearings," Tribol. Trans., in press.
[2] Chengwei, W., and Linqing, Z., 1989, "An Average Reynolds Equation for Partial Film Lubrication With a Contact Factor," J. Tribol., **111**, pp. 188–191.
[3] Patir, N., and Cheng, H. S., 1978, "Application of Average Flow Model to Lubrication Between Rough Sliding Surfaces," J. Lubr. Technol., **101**, pp. 220–230.
[4] Segal, A., 1993, "SEPRAN Users Manual," Technical Report, Ingenieursbureau SEPRA, Leidschendam, The Netherlands.
[5] Kovalchenko, A., Ajayi, O., Erdemir, A., Fenske, G., and Etsion, I., 2005, "The Effect of Laser Surface Texturing on Transitions in Lubrication Regimes during Unidirectional Sliding Contact," Tribol. Int., **38**, pp. 219–225.
[6] Burstein, L., and Ingman, D., 1999, "Effect of Pore Ensemble Statistics on Load Support of Mechanical Seal With Pore-Covered Faces," J. Tribol., **121**, pp. 927–932.
[7] Ronen, A., Etsion, I., and Kligerman, Y., 2001, "Friction-Reducing Surface-Texturing in Reciprocating Automotive Components," Tribol. Trans., **44**(3), pp. 359–366.
[8] Brizmer, V., Kligerman, Y., and Etsion, I., 2003, "A Laser Textured Parallel Thrust Bearing," Tribol. Trans., **46**(3), pp. 397–403.
[9] Siripuram, R. B., and Stephens, L. S., 2004, "Effect of Deterministic Asperity Geometry on Hydrodynamic Lubrication," J. Tribol., **126**, pp. 527–534.
[10] Etsion, I., 2005, "State of the Art in Laser Surface Texturing," J. Tribol., **127**, pp. 248–253.
[11] Feldman, Y., Kligerman, Y., Etsion, I., and Haber, S., 2006, "The Validity of the Reynolds Equation in Modeling Hydrostatic Effects in Gas Lubricated Textured Parallel Surfaces," J. Tribol., **128**, pp. 345–350.
[12] Brajdic-Mitidieri, P., Gosman, A. D., Loannides, E., and Spikes, H. A., 2005, "CFD Analysis of a Low Friction Pocketed Pad Bearing," J. Tribol., **127**, pp. 803–812.
[13] Arghir, M., Roucou, N., Helene, M., and Frene, J., 2003, "Theoretical Analysis of the Incompressible Laminar Flow in a Macro-Roughness Cell," J. Tribol., **125**, pp. 309–318.
[14] Sahlin, F., Glavatskih, S. B., Almqvist, T., and Larsson, R., 2005, "Two-Dimensional CFD-Analysis of Micro-Patterned Surfaces in Hydrodynamic Lubrication," J. Tribol., **127**, pp. 96–102.
[15] Ostayen van, R. A. J., 2002, "The Hydro-Support: An Elasto-Hydrostatic Thrust Bearing With Mixed Lubrication," PhD thesis, Delft University of Technology, Delft, The Netherlands.